AIAA

AIAA 97-0511

Boundary Layer Trips on Airfoils at Low Reynolds Numbers

C. Lyon, M. Selig, and A. Broeren
University of Illinois at Urbana-Champaign
Urbana, IL

35th Aerospace Sciences Meeting & Exhibit
January 6-10, 1997 / Reno, NV

BOUNDARY LAYER TRIPS ON AIRFOILS AT LOW REYNOLDS NUMBERS

Christopher A. Lyon,* Michael S. Selig,† and Andy P. Broeren*

Department of Aeronautical and Astronautical Engineering
University of Illinois at Urbana–Champaign
Urbana, Illinois 61801

Abstract

Three categories of boundary layer trips (single 2-D plain, multiple 2-D plain, and 3-D trips) were tested on the M06-13-128, E374, and SD7037 airfoils over the Reynolds numbers of 100,000 to 300,000. Flow visualization and drag data were acquired for a number of trip heights and locations. To facilitate comparisons between airfoils, trips were located relative to untripped laminar separation locations. Drag data showed dramatic drag reductions for relatively thin trips, with thicker trips having slightly better performance. The trip location proved to be of little significance for trips located upstream of laminar separation. Little advantage was seen in utilizing multiple 2-D trips or complex 3-D trips over single 2-D trips. Finally, through the application of trips, it was not possible to improve the performance of an airfoil exhibiting large laminar separation bubbles over that of an untripped airfoil with small bubbles.

I. Introduction

At low Reynolds numbers, the presence of laminar separation bubbles often results in the increased drag seen on some airfoils. In an effort to mitigate these adverse effects and improve low Reynolds number airfoil performance, two principal approaches have been taken. First, by careful tailoring of the pressure distribution, bubble drag can be reduced through the introduction of early transition. A second well-known approach involves the use of mechanical turbulators (trip wires, plain trips, distributed grit roughness, zigzag tape, etc.) all of which tend to enhance the instability of the Tollmien-Schlichting waves that ultimately leading to turbulent flow. Any resulting benefit is believed to be attributable to the initiation of premature transition and the consequent reduction or elimination of the laminar separation bubble.

Although effective tailoring of pressure distributions is well established.[1,2,3,4] transition enhancement by means of boundary layer trips is much less understood. The

* Graduate Research Assistant. Student Member AIAA.

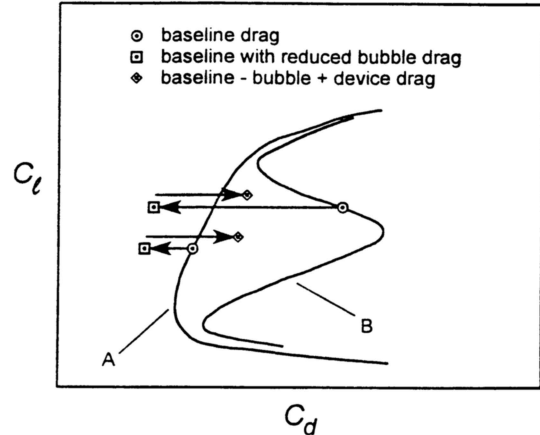†Assistant Professor. Member AIAA.

Fig. 1 Conceptual trip effects on an airfoil with low bubble drag (A) and an airfoil with high bubble drag (B).

countless combinations of trip geometries, sizes, and locations along the airfoil chord are daunting. Complicating the matter further, a particular configuration optimized for one airfoil may prove less favorable for another. Data gathered at Stuttgart,[5] Notre Dame,[6,7,8] Delft,[9] and elsewhere[10,11] show that, with some certainty, it may only be said that trips must be located in the vicinity of the bubble to be potentially effective.

Trip effectiveness is a consequence of three cumulative effects: added trip device drag, changes in bubble drag (pressure drag), and changes in skin friction drag, with the magnitude of each being airfoil dependent. The addition of a trip to an airfoil with a large bubble typically creates a large drag reduction due to the reduction in bubble drag, which is relatively large as compared with the increase in drag due to trip device drag and additional skin friction drag. Conversely, for airfoils with small bubbles, trips typically result in more device and skin friction drag than reductions in bubble drag. These effects are shown conceptually in Fig. 1 for large and small bubble airfoils. While a greater drag reduction is possible for airfoils with large laminar separation bubbles, it is unclear whether or not the drag produced would be less than that for untripped airfoils with small bubbles.

For the sake of clarity, skin friction effects were purposefully omitted from Fig. 1. Perhaps the simplest method of bringing to light skin friction effects is by assuming the use of an ideal trip that produces no device

drag yet retains its effectiveness in promoting transition. While such an ideal trip geometry may have excellent potential to increase airfoil performance, the remaining difficulty is finding the optimum trip location. For example, it could be placed such that the disturbances initiate transition well upstream of the bubble. While this consequently eliminates the bubble, unnecessarily large regions of turbulent flow (increased skin friction drag) are produced. By moving the trip closer to the bubble, transition could be forced to occur at the leading edge of the bubble and thereby reduce the amount of turbulent flow. This simple example highlights two important parameters that determine trip efficiency: trip geometry and trip location.

Though advances have been made in the understanding of boundary layer trips, considerable difficulty still surrounds the prediction of their effects even on flat plate boundary layers.[12,13] Airfoil effects such as surface curvature, pressure gradients, and transition through laminar separation bubbles further add to this difficulty, clearly hindering the formulation of a practical theory for low Reynolds number airfoils with trips. Moreover, the myriad of experiments on airfoils with trips,[5,6,7,8,9,14,15,16] though quite interesting and useful, have primarily focused on improving the performance of particular airfoils without providing insight into underlying trends. Consequently, progress in the understanding of boundary layer trips on airfoils will likely rely on new experimental data taken systematically over a wide range of parameters.

In an effort to fill this niche, an experimental investigation was conducted to provide data on three low Reynolds number airfoils with a range of trip configurations. In particular, emphasis was placed on obtaining detailed, quantitative data for comparative purposes. The three airfoils tested included the M06-13-128, E374, and SD7037, each being selected based on their respective bubble sizes (large to small) as determined from experimental performance data and predictions of pressure distributions from XFOIL.[17] While emphasis was placed on using easily replicated and installed 2-D trips, more complex trip geometries and configurations were studied as well in light of their favorable results discussed in the literature. In this regard, single trips, multiple trips,[18,19,20,21] (one after another), and several 3-D trips[9,22,23] were studied in detail.

II. Experimental Techniques

Only a brief discussion of the experimental apparatus and measurement techniques is presented. More details regarding the wind tunnel, the present setup, and the data acquisition and reduction process can be found in Ref. 24. All experiments were performed in the Uni-
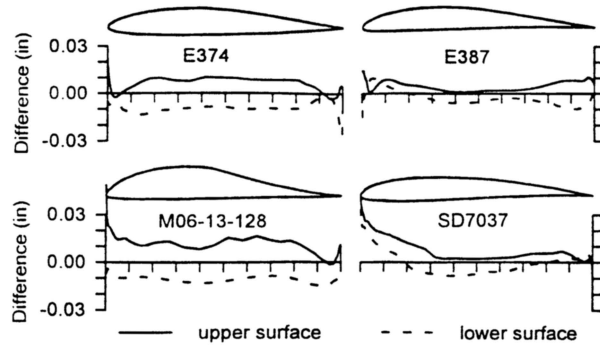

Fig. 2 Wind tunnel model accuracies for the E374, E387, M06-13-128, and SD7037 airfoils.

versity of Illinois at Urbana–Champaign (UIUC) open-return subsonic wind tunnel having a 2.8 × 4 ft rectangular test section. Owing to the low Reynolds numbers of the tests, test-section speeds ranged from 7–34 mph. In the empty test section, the turbulence level was measured to be less than 0.1% over the tunnel operating range.

All airfoil models tested had a 33 $\frac{5}{8}$-in. span and 12-in. chord. To isolate the ends of the model from the tunnel side-wall boundary layers and support hardware, models were mounted horizontally between two $\frac{3}{8}$-in. thick, 6-ft. long Plexiglas splitter plates. Gaps between the model and Plexiglas were nominally 0.05 in.

Airfoil model accuracy was determined using a Brown & Sharpe coordinate measuring machine. The measured coordinates were compared with the true coordinates using a least squares approach yielding average model accuracies of approximately 0.011 in. or better for the three models tested. The model accuracy plots, shown in Fig. 2, depict the differences in shape between the true airfoil and actual airfoil for the upper (solid line) and lower surface (dotted line).

The data acquisition process, being completely automated, used the momentum deficit method to determine drag. Owing to spanwise variations in drag at low Reynolds numbers,[24,25] wake-profile measurements were taken at 12 spanwise stations spaced 0.5 in. apart over the center 5.5 in. of the model span. After the resulting 12 values were corrected for solid blockage, wake blockage, streamline curvature[26] and circulation effects,[27] they were averaged to obtain drag coefficients accurate to within 2 counts ($\Delta C_d = 0.0002$).

The validation of the laminar separation and turbulent reattachment locations was determined through comparison of surface oil flow visualization features taken on a model of the E387 (Fig. 1) with those obtained from the NASA Langley Research Center Low-Turbulence Pressure Tunnel (LTPT).[28] The technique involved using a fluorescent pigment suspended in light
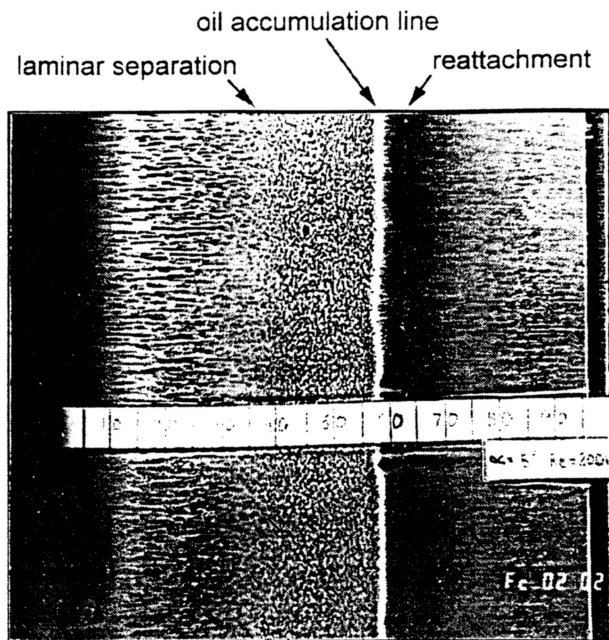
Fig. 3 Surface oil flow visualization on the E387 identifying major bubble features for $Re = 200{,}000$ and $\alpha = 5$ deg.

Fig. 4 Comparison of major bubble features on the E387 between UIUC and LTPT for $Re = 200{,}000$.

oil that was airbrushed onto the surface of the model. After 30–45 min. of continuous wind-tunnel run time, discernible surface flow features could be seen under a fluorescent light. Figure 3 shows a photograph of the fluorescent oil flow for $\alpha = 5$ deg and $Re = 200{,}000$ with key flow features identified. Data taken over a range of angles of attack are shown in Fig. 4 and compared with data from the LTPT. As seen, the agreement between the UIUC and LTPT laminar separation locations and oil accumulation lines is mostly within 1–2% of chord. It should be noted that the feature identified as reattachment in the LTPT experiment is labeled here as the "oil accumulation line." For higher dynamic pressures, such as in the Langley study, the faint features produced by reattachment (see Fig. 3) can quickly vanish during the tunnel run time, leaving the prominent oil accumulation line to be mistaken for reattachment.

To better understand the circumstances leading to the oil accumulation line, it is instructive to consider the skin friction coefficient distribution through the bubble. Time-averaged predictions of the skin friction coefficient distribution[29,30,31,32,33] show a narrow negative spike in the c_f distribution immediately upstream of reattachment. In this region, the oil is scrubbed forward until the resulting surface tension produced by the oil pool balances the shear stress imposed by the flow field, thereby leaving a line of accumulated oil. Between this line and the laminar separation line there is no oil movement as deduced from the negligible differences in surface oil flow
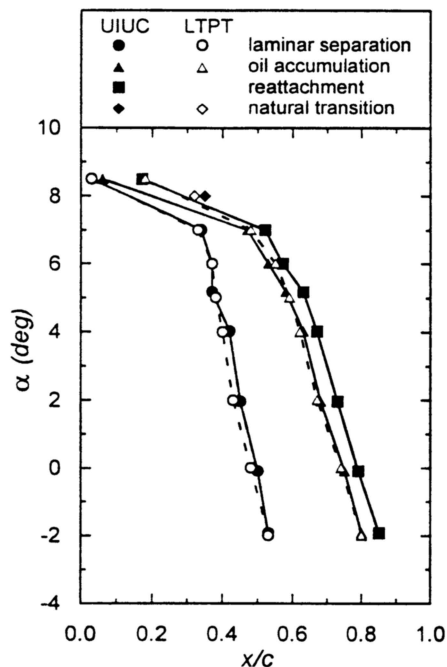
patterns before and after the 30–45 min. wind-tunnel run. Specifically, the oil in this region has an "orange-peel" texture, which is characteristic of freshly sprayed oil.

III. Results and Discussion
Untripped Data

To aid in data interpretation, baseline (untripped) drag for each of the three airfoils was gathered over a range of Reynolds numbers. Because of the time consuming nature of the experiments, generation of complete drag polars for each trip configuration was impractical. Therefore, the collection of data was limited to a single angle of attack selected for each airfoil. These angles of attack were 6.5, 3, and 2.2 deg for the M06-13-128, E374, and SD7037, respectively. Each angle of attack was chosen to correspond approximately to the middle of the drag polar for the respective airfoil.

Surface flow visualization was performed on all three airfoils to determine the laminar separation and turbulent reattachment locations over a range of Reynolds numbers. For later reference, the results are given in Table 1 together with the predictions of XFOIL[17] for comparison. Low surface shear stresses for $Re = 100{,}000$ and $150{,}000$ made identification of these features difficult, in which case this data is not included in the table. The small, relatively low-drag bubble on the SD7037 produced only subtle surface flow features that did not permit identification of laminar separation and reattachment.

3

Table 1: Separation and reattachment locations from surface flow visualization and predictions.

| | $Re = 200{,}000$ | | | |
| | Exp. | | XFOIL* | |
	x_S	x_R	x_S	x_R
M06-13-128	26	47	37	58
E374	43	72	47	70
SD7037	-	-	51	73
	$Re = 300{,}000$			
	Exp.		XFOIL*	
	x_S	x_R	x_S	x_R
M06-13-128	35	57	39	56
E374	44	67	48	66
SD7037	-	-	54	66

*Predictions using XFOIL Version 6.2 with $n = 9$

Fig. 5 Trip locations on the E374, SD7037, and M06-13-128 airfoils.

Trip Locations and Conventions

In order to facilitate comparisons of trip effectiveness on the three airfoils, all trips were located relative to laminar separation locations as predicted by XFOIL. The first trip location (closest to the bubble) was 0.1 in. upstream of the predicted bubble. Succeeding trips where then located 1 in. further upstream along the 12-in. chord airfoil surface. Unless otherwise noted, the trailing edge of all trips was used as the datum line. For instance, the trailing edge of the first trip (location 1) was 0.1 in. upstream of the predicted laminar separation point. Figure 5 shows each airfoil with the various possible trip locations. The few exceptions to these conventions will be explicitly stated in context with the results.

Single 2-D Plain Trip Data

The single 2-D trips discussed in this section consisted of a rectangular tape strip located according to Fig. 5. All tape trips were constructed by laminating together several layers of 0.002-in. thick, 0.5-in. wide adhesive
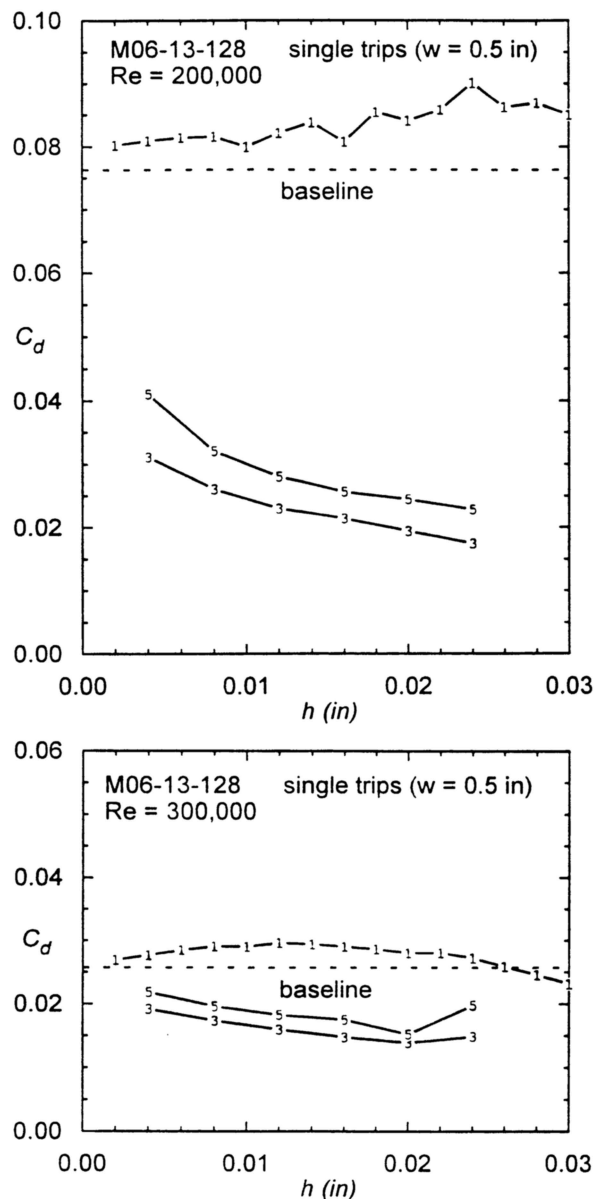

Fig. 6 M06-13-128 drag data for single 2-D plain trips of varying thickness at a) $Re = 200{,}000$ and b) 300,000.

tape (3M Scotch Brand C-4210 Removable Magic Tape). All data was obtained with the thickest trip configuration first, and then by removing successive layers of tape, data for lower trip heights were acquired. To prevent confusion when later comparing between single and multiple trips, all single-trip configurations are referred to by their locations as indicated in Fig. 5 with an "S" as the suffix. For example, 3S denotes a single trip of arbitrary height at location 3.

Figures 6a,b show data taken on the M06-13-128 for several trip heights and locations at $Re = 200{,}000$ and 300,000. Baseline (untripped) drag values for each Reynolds number have been plotted as dotted lines for

easy reference. In the plot, the character '1' is used as the symbol for trip 1S data, '3' for 3S, and '5' for 5S. Beginning with trip 1S, the drag has increased for a majority of the thicknesses tested at both Reynolds numbers. Upon comparison of location 1 with the clean bubble location obtained from flow visualization, it was found that XFOIL predicted laminar separation to be upstream of its true location (see Table 1). As a result, trip 1S was submerged within the bubble. This being the case, all 1S trip heights produced negligible effects on overall drag. It is interesting to note that for $Re = 300,000$, a reduction in drag was seen for the thickest trips tested ($0.026 \leq h \leq 0.030$ in.). In these cases, the trip height likely protruded through the separation streamline of the bubble, thereby having a more favorable influence on promoting transition and shortening the bubble.

As the trip was moved forward to location 3 on the M06-13-128. drag decreased dramatically for both Reynolds numbers at all trip heights. Of particular interest is the substantial drag reduction for the relatively thin trips. For the 0.004-in. thick trip, drag reductions were approximately 59.2% and 25.2% of the baseline drag values at $Re = 200,000$ and 300,000, respectively. Thus, flow disturbances leading to early transition are produced by extremely small protuberances. As the trip height was increased, device drag increased. but the larger disturbances shortened the bubble and resulted in lower total drag. Minimum drag was reached only for $Re = 300,000$ at a trip height of 0.020 in. At this point, reductions in bubble drag are likely offset by increases in skin friction and device drag.

Moving the trip forward to location 5 on the M06-13-128 produced no noticeable trend changes over those found for trips at location 3. Again. for $Re = 300,000$, minimum drag was found for $h = 0.020$ in. These minimums (found only for $Re = 300,000$) suggest that as the Reynolds number is increased the optimum trip heights become smaller, as expected. Surprisingly, the drag at all trip heights and Reynolds numbers was everywhere larger for trip 5S when compared with trip 3S. These results would seem appropriate had the bubble been eliminated by trip 3S since in that case trip 5S, being further upstream, would only contribute higher skin friction drag since no further reduction in bubble drag would be possible. The bubble, however. was not eliminated in either the 3S or 5S case as deduced by the decreasing drag with increasing trip height.

The exact reason why trip 5S produced higher drag than trip 3S cannot be determined from the data collected. It is speculated, however. that while trip 5S might have reduced bubble drag, increases in device and skin friction drag dominated. For airfoils such as the M06-13-128, however. where bubble drag dominates, changes in skin friction drag due to a shortened bubble should be negligible.

The effect of single trips on the E374 was studied for locations 1, 3, and 5. The Reynolds numbers tested were 100,000, 150,000, 200,000, and 300,000. and the data obtained is shown in Figs. 7a–d. It should be noted that the drag axis has been magnified to four times that of the previous M06-13-128 plots. Trip 1S was again submerged within the bubble and therefore produced negligible improvements over baseline drag values for all Reynolds numbers.

As the trip was moved to location 3 on the E374, results similar to those obtained on the M06-13-128 were seen at all Reynolds numbers except for $Re = 300,000$. Very small trip heights produced large drag reductions, with drag then decreasing as the trip height increased. An optimum trip height was not found at any of the Reynolds numbers over the range of trip heights tested except for $Re = 300,000$, supporting the previous conclusion that higher Reynolds numbers favor lower trips. For comparison, trip 3S with $h = 0.024$ in. and $Re = 200,000$, produced only a 13.1% drag reduction in drag as compared with the 59.2% reduction for the M06-13-128. The E374 benefits less since the bubble drag, which is reduced by the trip, represents a smaller contribution to the overall drag as compared with the M06-13-128 that has relatively large bubble drag.

By moving the trip further upstream on the E374 to location 5, no further significant drag reductions were produced at the Reynolds numbers tested. These results prompted an investigation into how far a single trip should be located from the bubble to reach maximum effectiveness. In this study, a narrow, moderate thickness trip ($w = 0.125$ in., $h = 0.013$ in.) was made from a strip of mylar and affixed to the model with double sided tape. Figures 8a–c show the effect of moving the trip upstream for $Re = 100,000$, 200,000, and 300,000. Again. the baseline drag has been shown as a dotted line. The x-axis is such that $s = 0$ in. corresponds to trip location 1 and $s = 4$ in. corresponds to trip location 5. Thus, upstream values of s tend toward the left side of the s-axis. As the data shows. dramatic drag reductions occurred near $s = 1$ in. for all Reynolds numbers. Upon comparison of this data with the laminar separation locations obtained from flow visualization. $s = 1$ in. corresponds to the beginning of the bubble. The drag reduction, therefore, was a result of moving the trip forward and out of the bubble. For any location further upstream. there is relatively little change in drag except for $Re = 300,000$ for which case the increased device and skin friction drag dominated for the upstream trip locations. It should be noted that no significant differ-
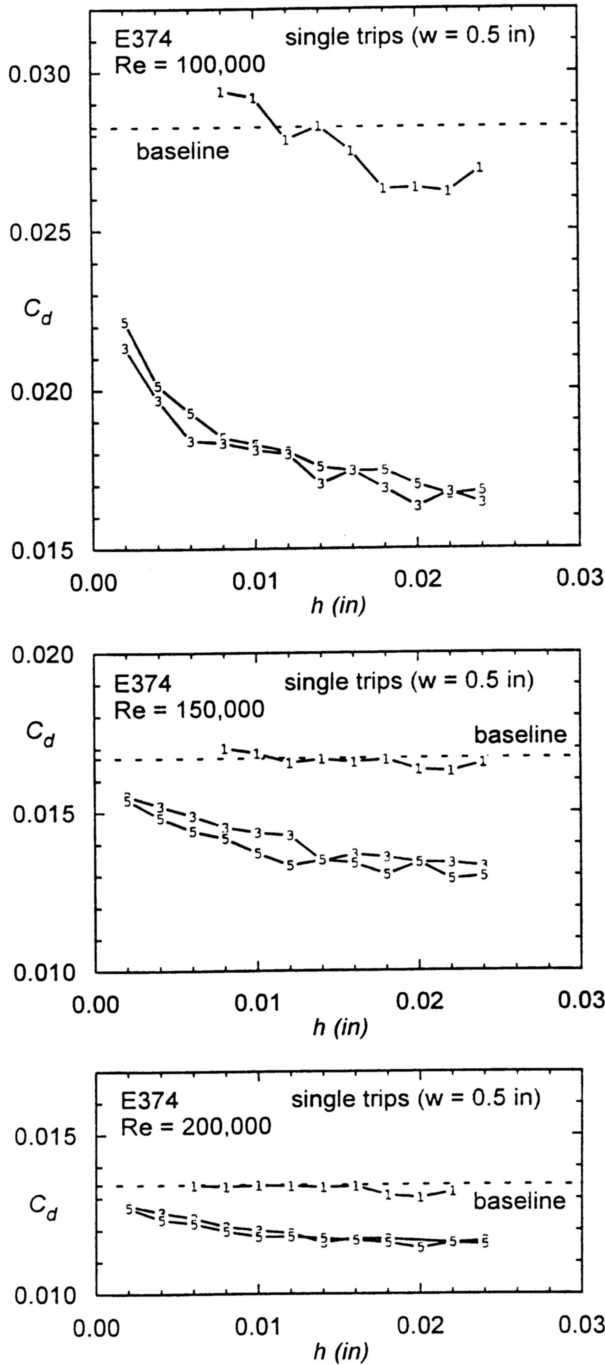
Fig. 7 E374 drag data for single 2-D plain trips of varying thickness at a) $Re = 100,000$, b) 150,000, c) 200,000, and d) 300,000. (figure continues)

ences in drag were produced by changes in trip width as long as the trip trailing edges coincided (see Fig. 9 for trip 3S). These results support the conclusions of others that the trip trailing edge introduces the key disturbances that lead to transition.

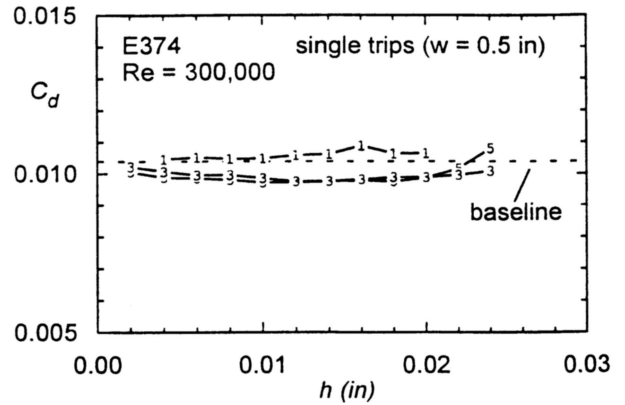From an applications standpoint, this trip location data provides two important pieces of information.

Fig. 7 Continued.

First, a trip placed far upstream relative to the bubble exhibits no advantage over one placed relatively close. This would dictate placing the trip as far forward as possible to eliminate any possibility of submerging the trip within the bubble at other angles of attack. Second, trip performance is relatively insensitive to changes in trip widths, thereby allowing for the use of the most convenient trip width without any drag penalty.

Drag measurements shown in Fig. 10 were taken on the SD7037 at $Re = 200,000$. Unlike the other two airfoils that exhibited large reductions in drag with small trip heights due to reductions in bubble sizes, the SD7037 displayed little effect except at large trip heights where device drag began to dominate. These data suggest that an airfoil designed to exhibit short laminar separation bubbles does not benefit from the addition of single 2-D trips.

Multiple 2-D Plain Trip Data

In this study, multiple trips consisted of several plain trips simultaneously placed at adjacent locations as specified in Fig. 6. The multiple trips will be referred to by the most upstream trip location with an "M" as the suffix. For instance, 3M signifies trips located at locations 1, 2, and 3, which were 0.1 in., 1.1 in., and 2.1 in. upstream of the predicted laminar separation location.

Figures 11a,b show trip data collected for trips 1M, 3M, and 5M on the Miley at $Re = 200,000$ and 300,000. It should be noted that trips 1M and 1S are the same configuration. At $Re = 200,000$, an extremely broad low-drag range (with trip thickness) was present for trip 3M. This relatively constant drag with increased trip thickness is likely caused by a lower bubble drag accompanied by higher device drag — the resulting effect of which nets little gain.. Comparison between trips 3S and 3M showed a slightly lower drag for 3M over the range of thicknesses tested. This suggests that any increases in device drag due to the introduction of multiple trips was offset by increased flow disturbances leading to reduced bubble drag. As the Reynolds number was increased to
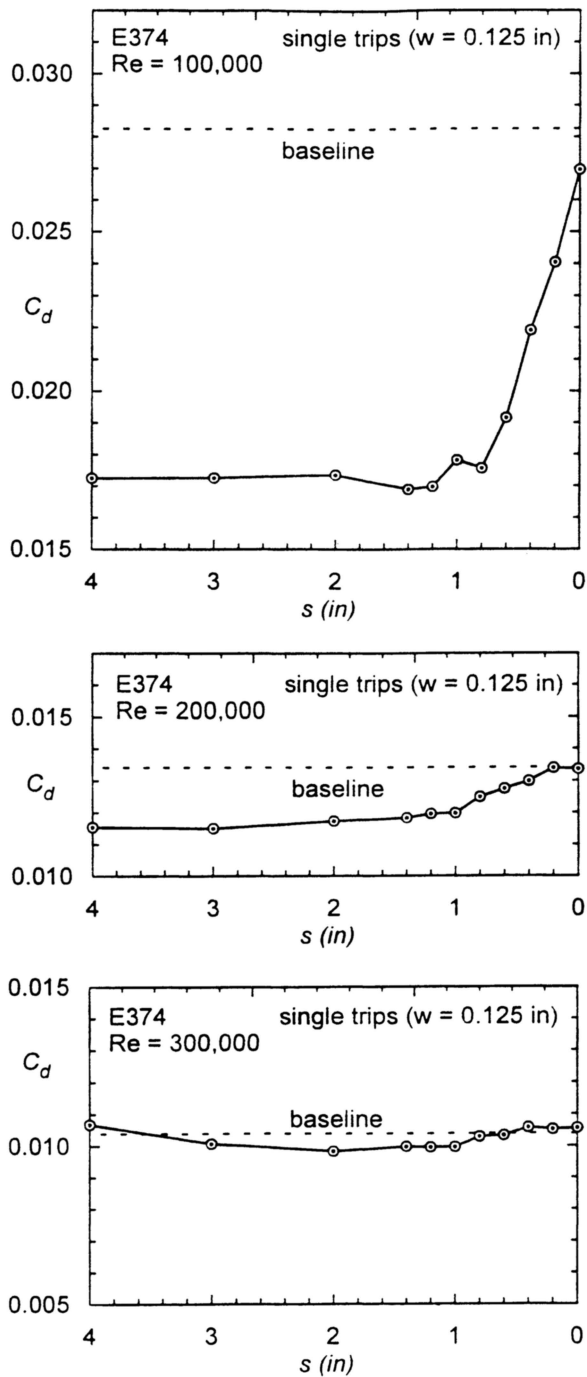
6

Fig. 8 E374 drag data for single 2-D plain trips ($w = 0.125$ in.. $h = 0.013$ in.) at various streamwise locations for a) $Re = 100,000$. b) 200,000. and c) 300,000.
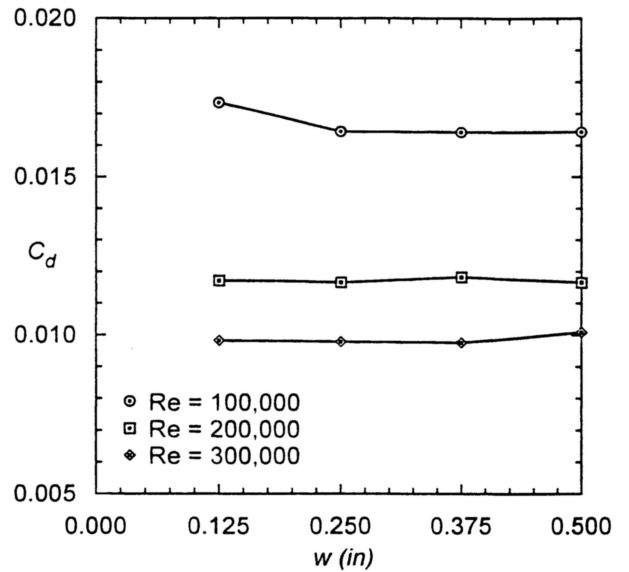

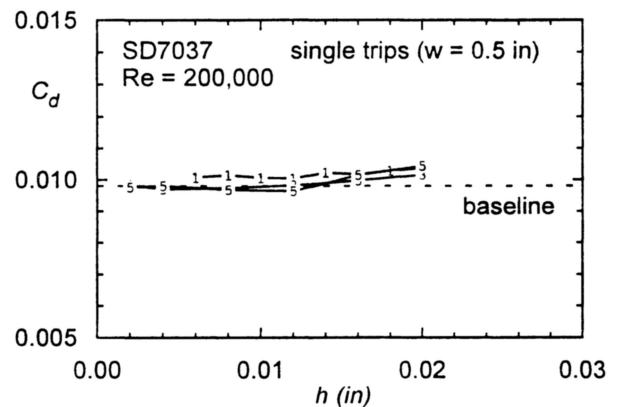Fig. 9 E374 drag data at various Reynolds numbers for single 2-D plain trips of varying widths ($h = 0.013$ in.).

Fig. 10 SD7037 drag data for single 2-D plain trips of varying thickness at $Re = 200,000$.

300,000. a minimum was seen for trip 3M. It is interesting to note that the minimum occurred at a smaller height ($h = 0.014$ in.) as compared with trip 3S at the same Reynolds number (see Fig. 6b).

Flow visualization was performed at $Re = 300,000$ for trip 3M with $h = 0.013$ in. on the M06-13-128, and the

results are shown in Fig. 12. The flow visualization displayed no evidence of a bubble. which is supported by Fig. 11b showing minimum drag near $h = 0.013$ in. For any trips thinner than this, a bubble appears and generates higher drag. For thicker trips, increases in device drag pushes the overall drag to higher values. A feature of this flow visualization that may be misleading is the apparent presence of separated flow toward the trailing edge as evident by the orange-peel oil texture. This feature, however. is due to very low skin friction resulting from the Stratford-type pressure recovery. Also, it appears as if an oil accumulation line has formed near 50% chord. Again. this is not the case since the oil was being scrubbed in the downstream direction during the test run. Had the run continued, this line would have slowly moved further downstream.
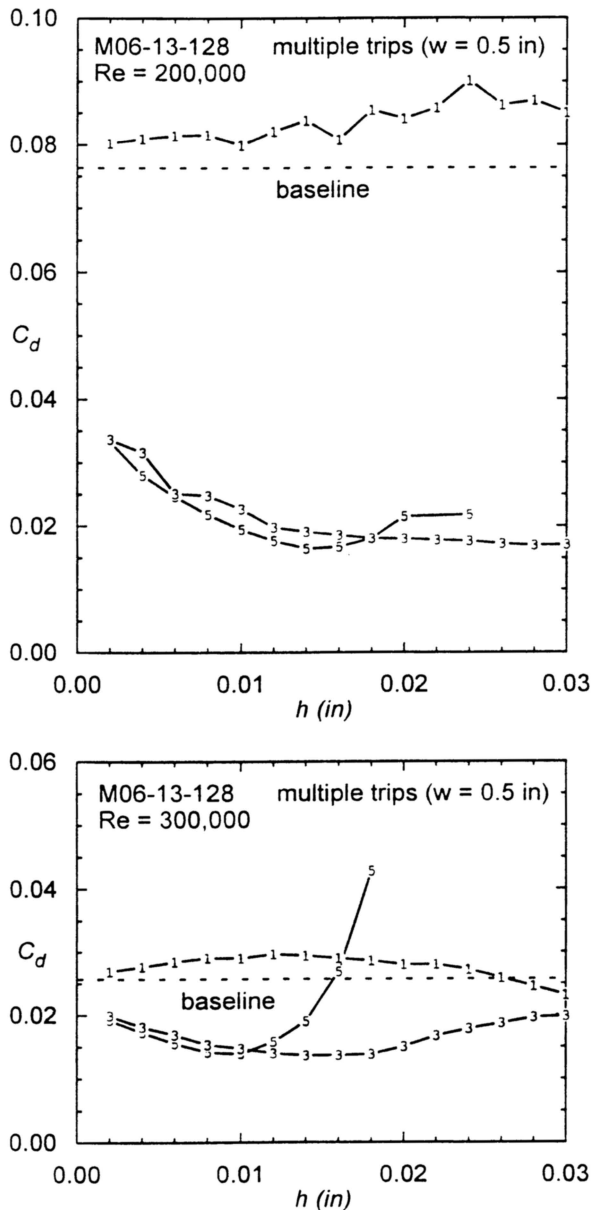
Fig. 11 M06-13-128 drag data for multiple 2-D plain trips of varying thickness at a) $Re = 200,000$ and b) 300,000.

Trip 5M showed a distinct minimum for both Reynolds numbers on the M06-13-128 and produced lower drag than trip 5S for similar heights. Again, increased device drag was likely offset by reduced bubble drag. The increase in device drag produced by adding more trips becomes apparent when trips 3M and 5M are compared for $h = 0.014$ in. As flow visualization showed for a trip height very similar to this, the bubble was eliminated by trip 3M. Therefore, the addition of more trips would only serve to increase device drag. The data supports this by showing higher drag for trip 5M. For the lower trip heights, however, the increased distur-
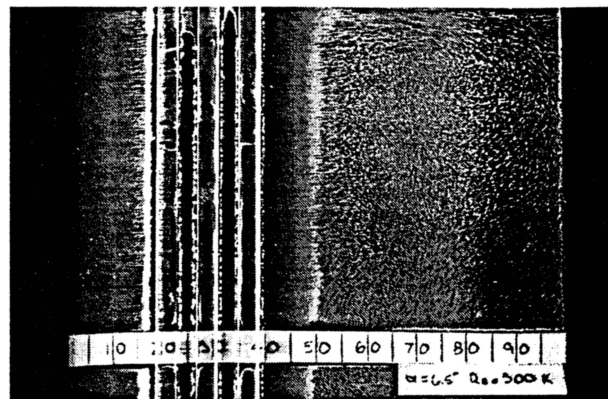

Fig. 12 M06-13-128 flow visualization for trip 3M ($h = 0.013$ in.) at $Re = 300,000$.

bances produced by 5M offset any penalty produced by increased device drag and thereby lead to lower overall drag as compared with trip 3M for similar heights.

Multiple trips were tested on the E374 for all five locations for $Re = 100,000, 150,000, 200,000$. and 300,000. These data are shown in Figs. 13a–d. In general, increasing the number of trips reduced drag at all Reynolds numbers, being particularly effective at $Re = 100,000$ where a maximum drag reduction of 43.2% occurred for trip 5M at $h = 0.014$ in. Again, an increase in the number of trips produced larger device drag that was then offset by larger reductions in bubble drag.

Comparisons of this multiple trip data with the single trip data for the E374 leads to more interesting results. For $Re = 100,000$, trip 3M produced higher drag than trip 3S while the opposite was true for location 5 where trip 5M produced lower drag than trip 5S. As deduced from the decreasing drag with increasing trip height, the bubble was not eliminated in any of these cases. One would therefore be tempted to expect a reduction in drag as more trips were added as a result of a shortened bubble. Clearly, a drag reduction was not present between trips 3S and 3M or trips 3M and 5M.

As the Reynolds number was increased from 150,000 to 300,000, three distinct trends were seen on the E374. Note that in each case, trip 2M was at the leading edge of the bubble thereby making a comparison with the other trips difficult. First, for $Re = 150,000$, trip 5M produced nearly the same effect as trip 5S, yet trip 3M had slightly lower drag than trip 3S. These results are a reversal of what was seen for $Re = 100,000$. At $Re = 200,000$, all trips performed nearly the same excluding trip 2M for reasons stated above, and not until $Re = 300,000$ was any significant variation seen between trip configurations. Trip 5M eliminated the bubble and produced excessive device drag for the thicker trips tested.

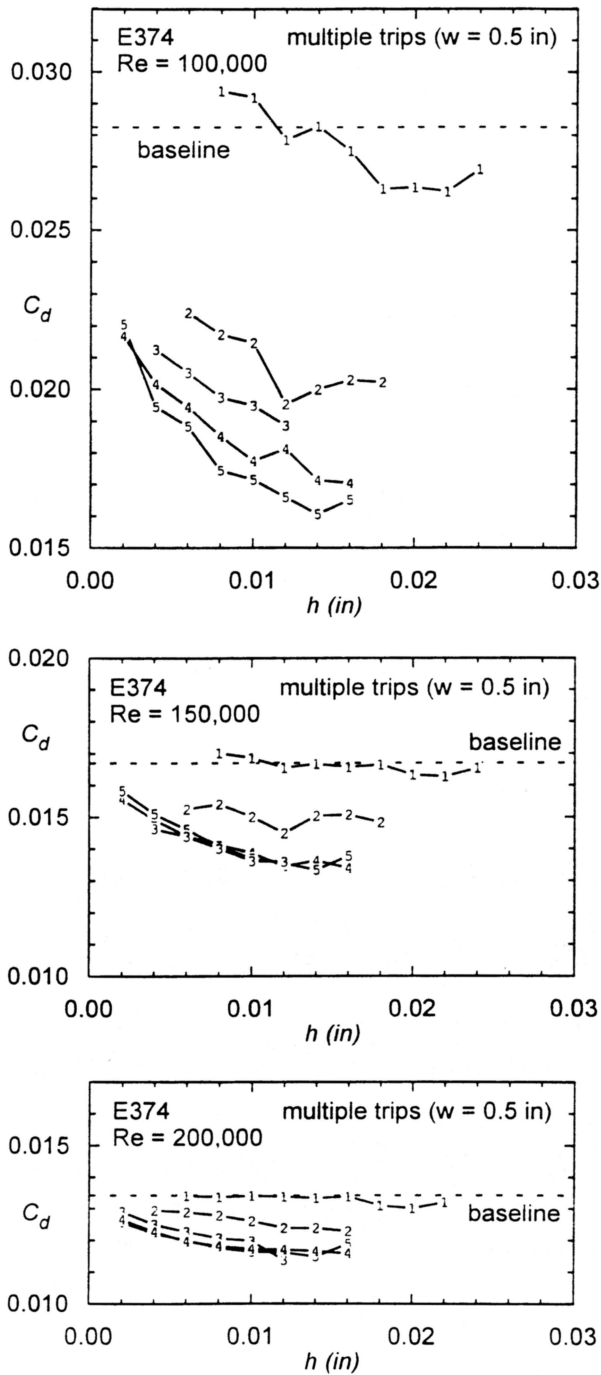Figure 14 shows data taken on the SD7037 with mul-

Fig. 13 Continued.

Fig. 14 SD7037 drag data for multiple 2-D plain trips of varying thickness at $Re = 200,000$.

Fig. 13 E374 drag data for multiple 2-D plain trips of varying thickness at a) $Re = 100,000$, b) 150,000, c) 200,000. and d) 300,000. (figure continues)

tiple trips 1M, 2M, 3M, 4M, and 5M for $Re = 200,000$. As with the single trip cases (Fig. 10), the addition of trips had no beneficial effect.

3-D Trip Data

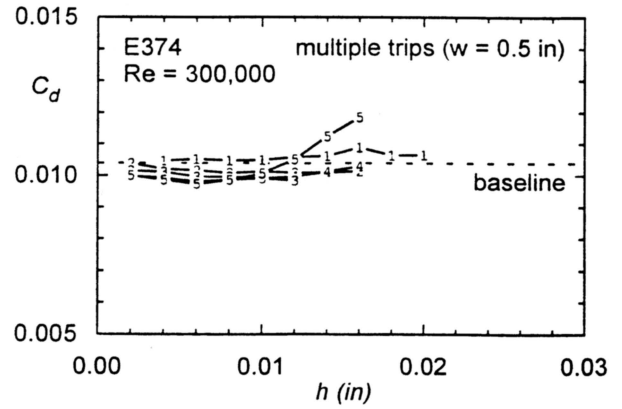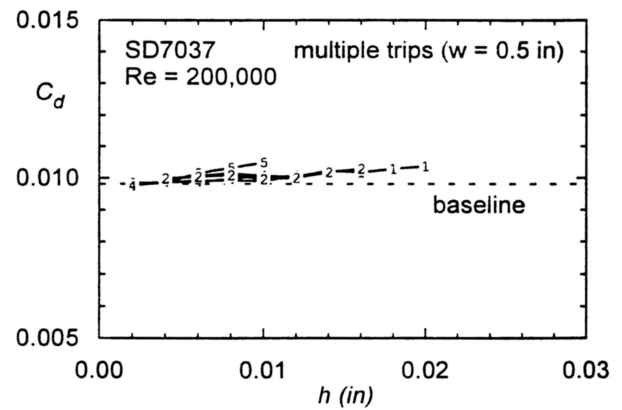Several styles of 3-D trips (triangular patches – call here "Hama" trips, [22,23] conventional zigzag, crescent zigzag, and raised hemisphere trips) were tested on the E374 for $Re = 200,000$. The geometries tested are shown in Fig. 15 along with the datum lines used when positioning. All trips were tested at location 3. Because of the difficulty in constructing repeatable, 3-D shapes, only a limited number of heights were tested, all tending toward moderate thicknesses. Also, because the construction technique and material was not always similar between the trips, it was not always possible to construct trips of similar heights.

Figure 16 shows the drag that each configuration produced as well as baseline drag and that for the 2-D plain trips 3S and 3M. The data suggests that large features were favored over smaller ones. For example, the wide zigzag and large Hama trip produced lower drag than did the smaller versions of these trips. It also appears as if the variation in trip performance with thickness was geometry dependent. The crescent zigzag trip, which was quite similar in geometry to the smallest (narrow and medium) zigzag trips, produced a reduction in drag for $h = 0.026$ in. while the smallest zigzag trips resulted in a drag increase. Flow visualization was performed
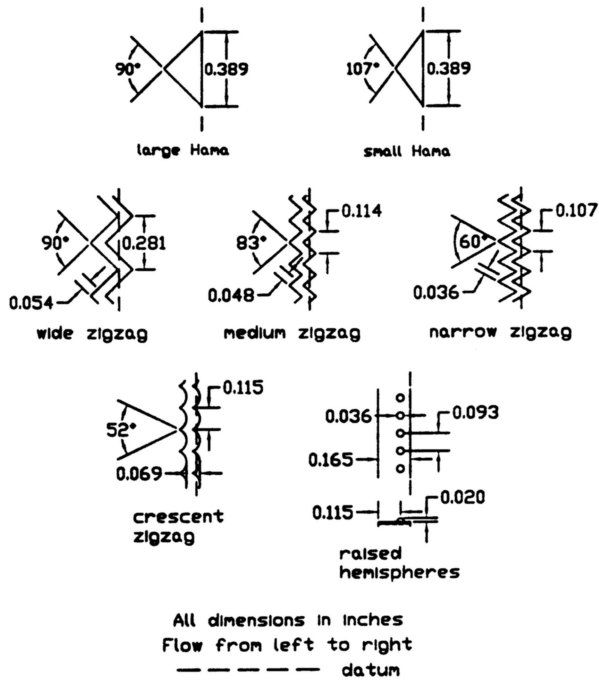
Fig. 15 The 3-D trip configurations tested.

Fig. 16 E374 drag data for 3-D trips of varying thickness at $Re = 200{,}000$.

Fig. 17 Close up of E374 flow visualization for the wide zigzag trip with $h = 0.047$ in.

on the wide zigzag trips for $h = 0.030$ and 0.047 in. A closeup of the results is shown in Figs. 17 and 18, respectively. The thicker trip, while producing an extremely 3-D boundary-layer disturbance, showed no evidence of a bubble. It appears as if turbulent wedges formed immediately behind the downstream spike, with laminar flow present behind the upstream spike. Immediately behind the trip, small cellular regions of reversed flow formed and may have served to trip the flow and lead to the formation of the turbulent wedges. For the thinner zigzag trip (Fig. 17), a rather ambiguous region exists between the trip and the apparent formation of turbulent wedges. Whether this region contains a laminar separation bubble is unclear.

While flow visualization showed a quite different flow structure behind the zigzag trips as compared with the 2-D plain trips, 3-D trips exhibited little advantage over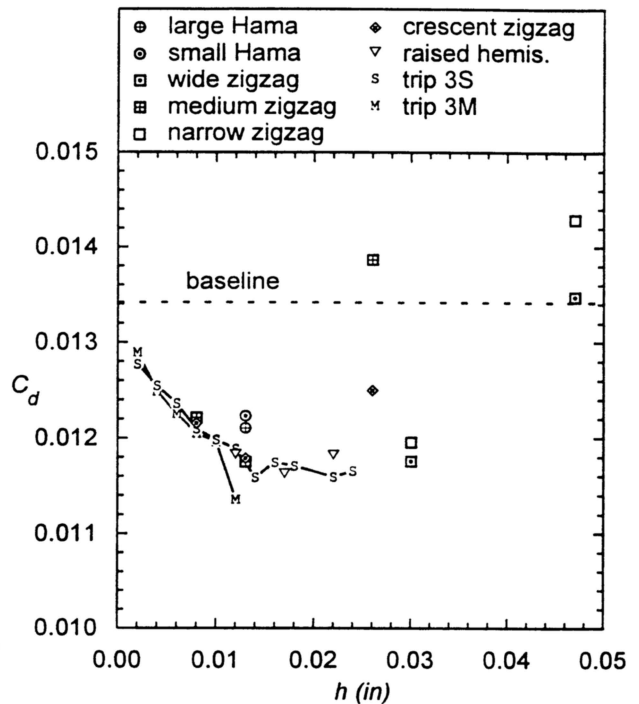 both the single or multiple 2-D plain trips. Again, from an applications standpoint, these data suggest that the use of 3-D trips on low-Reynolds number airfoils produces no clear benefit over 2-D plain trips.

IV. Conclusions

Extensive tests on several airfoils with a variety of trip configurations has lead to the following conclusions. First, it was shown that relatively thin trips are capable of producing fairly dramatic changes in drag for airfoils with large bubbles. Also, as trip heights increased, a broad range was seen where drag reduction was nearly constant. This was attributed to trade-offs made be-

10
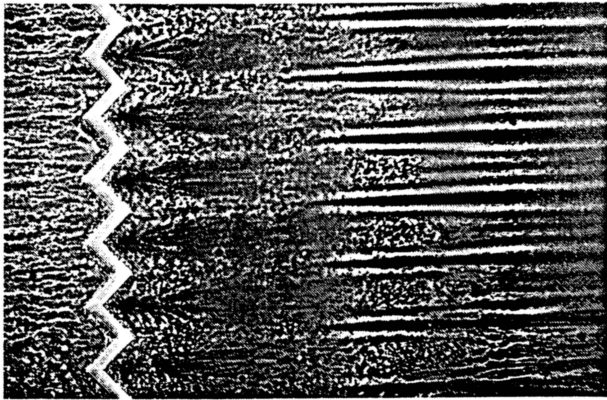
Fig. 18 Close up of E374 flow visualization for the wide zigzag trip with $h = 0.030$ in.

tween device drag, skin friction drag, and bubble drag. It was also shown that airfoils exhibiting large laminar separation bubbles benefited most from using boundary layer trips. No trip configuration, however, produced lower drag than a clean airfoil design to exhibit low bubble drag. Finally, multiple as well as 3-D trips were shown to produce no clear benefit over single 2-D plain trips.

Acknowledgments

References

[1] Wortmann, F.X.,, "Progress in the Design of Low Drag Airfoils," *Boundary Layer and Flow Control*, G.V. Lachmann (ed.), Pergamon Press. London, 1961, pp. 748–770.

[2] Maughmer, M.D. and Somers. D.M., "Design and Experimental Results for a High-Altitude, Long-Endurance Airfoil," *J. Aircraft*, Vol. 26, No. 2, 1989, pp. 148–153.

[3] Eppler, R., *Airfoil Design and Data*. Springer-Verlag, New York, 1990.

[4] Somers, D.M., "Subsonic Natural-Laminar-Flow Airfoils." *Natural Laminar Flow and Laminar Flow Control*, R.W. Barnwell and M.Y. Hussaini (eds.), Springer-Verlag, New York, 1992. pp. 143–176.

[5] Althaus. D., *Profilpolaren für den Modellflug—Windkanalmessung an Profilen im Kritischen Reynoldszahlbereich*. Neckar-Verlag Villingen-Schwenningen. Germany, 1980.

[6] Mueller, T.J., and Batill, S.M., "Experimental Stud-

ies of the Laminar Separation Bubble on a Two-Dimensional Airfoil at Low Reynolds Numbers," *AIAA J.*, Vol. 20, No. 4, 1982, pp. 457–463.

[7] Bloch, D.R., and Mueller. T.J., "Effects of Distributed Grit Roughness on Separation and Transition on an Airfoil at Low Reynolds Numbers," AIAA Paper 86-1788, 1986.

[8] Huber, A.F., II, and Mueller, T.J., "The Effect of Grit Roughness on the Performance of the Wortmann FX 63-137 Airfoil at a Chord Reynolds Number of 100,000," *Proceedings of the Aerodynamics at Low Reynolds Numbers $10^4 < Re < 10^6$ International Conference*, London, October 1986, pp. 28.1–28.16.

[9] Boermans, L.M.M., Duyvis, F.J.D., Ingen, J.L. van, and Timmer, W.A., "Experimental Aerodynamic Characteristics of the Airfoils LA 5055 and DU 86-084/18 at Low Reynolds Numbers," *Lecture Notes in Engineering: Low Reynolds Number Aerodynamics*, T.J. Mueller (ed.), Vol. 54, Springer-Verlag, New-York, June 1989, pp. 115–130.

[10] Schmitz, F.W., "Aerodynamik des Flugmodells, Tragflugelmessungen I," C.J.E. Volckmann Nachf. E. Wette, Berlin-Charlottenburg 2, 1942 ("Aerodynamics of the Model Airplane, Part I, Airfoil Measurements," translated by Redstone Scientific Information Center, U.S. Army Missile Command, Redstone Arsenal, Alabama, NASA TMX 60976, Nov. 1967) (NASA Accession Number N70-39001).

[11] Pfenninger, W., "Investigations on Reductions of Friction on Wings, in Particular by Means of Boundary Layer Suction," NACA TM 1181, August 1947.

[12] Nayfeh, A.H., and Ragab. S.A., "Effect of Roughness on the Stability of Boundary Layers," AIAA Paper 86-1044, May 1986.

[13] Danabasoglu, G. Biringen. S., and Streett, C.L., "Spatial Simulation of Boundary Layer Instability: Effects of Surface Roughness." AIAA Paper 93-0075, Jan. 1993.

[14] Selig, M.S.. Donovan, J.F., and Fraser, D.B., *Airfoils at Low Speeds*. SoarTech Publications, Virginia Beach, VA, 1995.

[15] Selig, M.S.. Guglielmo. J.J., Broeren, A.P., and Giguère, P., *Summary of Low-Speed Airfoil Data – Vol. 1*, SoarTech Publications, Virginia Beach, VA, 1995.

[16] Selig, M.S.. Lyon, C.A.. Giguère. P. Ninham. C.N., and Guglielmo. J.J., *Summary of Low-Speed Airfoil Data – Vol. 2*. SoarTech Publications, Virginia Beach, VA, 1996.

[17] Drela, M.. "XFOIL: An Analysis and Design System for Low Reynolds Number Airfoils." *Lecture Notes in Engineering: Low Reynolds Number Aerodynamics*, T.J. Mueller (ed.), Vol. 54, Springer-Verlag, New

York, June 1989, pp. 2–12.

[18] Pfenninger, W., "Experimental Investigation of an Airfoil with High Lift to Drag Ratios at Low Reynolds Numbers," Report No. BLC-84, Northrup Aircraft Inc., Feb. 1956 (NAI 560188).

[19] Carmichael, B.H., "Low Reynolds Number Airfoil Survey Volume I," NASA CR-165803, Nov. 1981.

[20] Mangalam, S.M., and Pfenninger, W., "Wind-Tunnel Tests on a High Performance Low-Reynolds Number Airfoil," AIAA Paper 84-0628, March 1984.

[21] Pressnell, M.S., "The Performance of Model Aircraft Using Flow Invigorators Gliding in the Critical Range of Reynolds Numbers," *Proceedings of the Aerodynamics at Low Reynolds Numbers $10^4 < Re < 10^6$ International Conference*, London, October 1986, pp. 32.1–32.32.

[22] Hama, F., "An Efficient Tripping Device," *J. of the Aeronautical Sciences*, Vol. 24, March 1957. pp. 236–237.

[23] Hegarty, J.G., and Hama, F.R., "Further Investigations on the Triangular-Patch Turbulator," University of Maryland, The Institute of Fluid Dynamics and Applied Mathematics, Technical Note BN-107 (AFOSR TN-57-616 & ASTIA AD 136 605), June 1957.

[24] Guglielmo, J.J., "Spanwise Variations in Profile Drag for Airfoils at Low Reynolds Numbers," Master's Thesis, University of Illinois at Urbana-Champaign, Dept. of Aeronautical and Astronautical Engineering, May 1996.

[25] Guglielmo, J.J. and Selig, M.S., "Spanwise Variations in Profile Drag for Airfoils at Low Reynolds Numbers," *Journal of Aircraft*, Vol. 33, No. 4, July–August 1996. pp. 699–707.

[26] Rae. W.H., Jr., and Pope, A., *Low-Speed Wind Tunnel Testing*, John Wiley and Sons. New York. 1984.

[27] Giguère. P. and Selig, M.S., "Freestream Velocity Measurements and Corrections for Two-Dimensional Testing with Splitter Plates," AIAA Paper 96-2388, June 1996.

[28] Evangelista, R., McGhee, R.J., and Walker, B.S., "Correlation of Theory to Wind-Tunnel Data at Reynolds Numbers below 500,000," *Lecture Notes in Engineering: Low Reynolds Number Aerodynamics*, T. J. Mueller (ed.), Vol. 54, Springer-Verlag, New York. June 1989. pp. 131–145.

[29] Lin, J.C.M., and L.L. Pauley, "Low-Reynolds-Number Separation on an Airfoil," *AIAA J.*, Vol. 34, No. 8. 1996. pp. 1570–1577.

[30] Pauley, L.L., and Hsiao. C.T., private communications. 1996.

[31] Walker. G.J., Subroto, P.H., and Platzer. M.F.. "Transition Modeling Effects on Viscous/Inviscid Interaction Analysis of Low Reynolds Number Airfoil Flows Involving Laminar Separation Bubbles," ASME 88-GT-32, June 1988.

[32] Kwon, O.K. and Pletcher, R.H., "Prediction of Incompressible Separated Boundary Layers Including Viscous-Inviscid Interaction," *Transactions of the ASME*, Vol. 101, Dec. 1979, pp. 466–472.

[33] Davis, R.L., and Carter. J.E., "Analysis of Airfoil Transitional Separation Bubbles," NASA CR-3791, 1984.